Experimental Validation of Compliance Zone at the Cerebral Arterial Bifurcation: Comparison Study with Reproducible Phantom and Computational Fluid Dynamics Simulation

Young-Jun Lee

Department of Medicine

The Graduate School, Yonsei University

Experimental Validation of Compliance Zone at the Cerebral Arterial Bifurcation: Comparison Study with Reproducible Phantom and Computational Fluid Dynamics Simulation

Directed by Professor Tae-Sub Chung

The Doctoral Dissertation
submitted to the Department of Medicine
the Graduate School of Yonsei University
in partial fulfillment of the requirements for the degree
of Doctor of Philosophy

Young-Jun Lee

June 2013

This certifies that the Doctoral Dissertation of Young-Jun Lee is approved.

Thesis Supervisor : Tae-Sub Chung

Thesis Committee Member#1 : Seung-Koo Lee

Thesis Committee Member#2 : Kook-Jin Ahn

Thesis Committee Member#3: Seung Kon Huh

Thesis Committee Member#4: Won Taek Lee

The Graduate School
Yonsei University

June 2013

ACKNOWLEDGEMENTS

First of all, I deeply appreciate Professor Tae-Sub Chung for the encouragement and guidance during my doctoral course. I also thank Professor Seung Kon Huh, Professor Won Taek Lee, Professor Seung-Koo Lee and Professor Kuk-Jin Ahn for giving me invaluable advices.

I would like to dedicate this thesis to my wife and lovely daughters who gave me full support and belief in my whole life.

June 2013

Young-Jun Lee

<TABLE OF CONTENTS>

LIST OF FIGURES

ABSTRACT

Experimental Validation of Compliance Zone at the Cerebral Arterial Bifurcation: Comparison Study with Reproducible Phantom and Computational Fluid Dynamics Simulation

Young-Jun Lee

Department of Medicine
The Graduate School, Yonsei University

(Directed by Professor Tae-Sub Chung)

A zone compliant to pulsatile flow (compliance zone) showing evagination-and-flattening at the apex of the cerebral arterial bifurcation was documented in our previous report using electrocardiogram-gated CT and MR angiography. We aimed to validate the existence of compliance zones and examine their relationship to local thin-elastic walls.

We examined different bifurcating vascular models; a phantom with a thin-elastic region at the apex, and computational fluid dynamics (CFD) models with either an elastic or rigid region at the apex of a bifurcation.

In the phantom, the elastic region at the apex of the bifurcation showed evagination-and-flattening in time with the pulsatile circulating fluids. The size of the evaginations increased when the outlet side was tilted down below the level of the flow-generating pump. Pulsatile evagination could be simulated in the CFD model with an elastic region at the bifurcation apex, and the pressure gradient was highest in the evaginating apex in peak systolic phase.

We were able to demonstrate a compliance zone, which responds to pressure gradients, experimentally, in the form of a thin-elastic region at an arterial bifurcation.

Key words: aneurysm, computational fluid dynamics, phantom, compliance

Experimental Validation of Compliance Zone at the Cerebral Arterial Bifurcation: Comparison Study with Reproducible Phantom and Computational Fluid Dynamics Simulation

Young-Jun Lee

Department of Medicine
The Graduate School, Yonsei University

(Directed by Professor Tae-Sub Chung)

I. INTRODUCTION

We have described periodic evagination-and-flattening at the apex of the cerebral arterial bifurcation accompanying the cardiac cycle on electro cardiogram (ECG)-gated MR and CT angiography in vivo, and we have designated it a compliance zone.[1] The walls of arteries are compliant to pulsatile flow patterns, which facilitates forward flow from the heart to far distant organs. More importantly, there exist regions with relatively thin walls at points of arterial bifurcation, which manifest as an absence of medial muscles and intermittent discontinuities of the internal elastic lamina.[2-5] These special regions are more compliant to pulsatile flow than the neighboring walls, as we have previously reported. Although compliance zones are not seen at every cerebral arterial bifurcation in every individual, they may be related to inherent characteristics of cerebral arterial bifurcations and are also consistent with the preferential sites of aneurysms. However, we noted a few discrepancies between ECG-gated CT angiograms and MR angiograms. Since, in MR angiography using time-of-flight (TOF) techniques, images can be falsely interpreted to have evaginations or aneurysms for various hemodynamic reasons, including flow signal loss by turbulence, flow-related enhancement, complex vasculature and

miscellaneous surrounding confusing signal intensities,[6-10] we needed to confirm the existence of the compliance zone observed in our previous study and its relationship with thin-elastic walls.

Phantom experiments and computational fluid dynamics (CFD) simulations have been widely used to evaluate the hemodynamics of cerebrovascular structures, because it is difficult to perform human studies in vivo.[11-14] Overall good agreement between phantom experiments and CFD simulations has been confirmed in many previous reports.[11, 15] If one could develop standard phantom and CFD models specifically designed to evaluate compliance zones, one might be able to reproduce and validate their existence. Moreover, such model systems could be valuable tools for future research into the origin of aneurysms.

We therefore aimed to validate the existence of compliance zones at the apex of bifurcations by 1) in vitro demonstration of compliance zone at bifurcations in phantom experiments and CFD simulations, 2) investigation of the relationship between compliance zones and thin-elastic walls, 3) identification of hemodynamic factors that produce evagination-and-flattening.

II. MATERIALS AND METHODS

The models we designed had a thin-elastic region at the apex of the bifurcation with similar characteristics to the medial defect region of the cerebral arterial bifurcation.

1. Phantom experiment

A. Phantom and pulsatile flow loop design

A home-made silicon phantom (Figure 1A) imitating a bifurcating vessel with a thin-elastic zone at the apex was constructed to evaluate morphological changes in response to pulsatile flow. The specifications of the phantom were as follows; luminal diameter (proximal inlet, 8mm; both distal outlets 6mm), bifurcation angle (140°), length of proximal parent segment before bifurcation (7cm) and distal branch segment after bifurcation (10cm), wall thickness at the apex (less than 0.3mm) and wall thickness of the remainder (1mm). In contrast to non-elastic walls, the elastic zone of the phantom was specially designed to possess elasticity by using different thickness and ingredients. The phantom is fixed to an acrylic box and connected to a computer-driven piston pump (UHDC, Ontario, Canada) programmed to create a pulsatile flow loop corresponding to normal human cerebral blood flow, by pumping forward at a systolic pumping volume of 30 ml (average, 9.196 ml) per second (Figure 1B). The working fluid in the model is a solution of water and glycerine (1: 1.4 mixture) of kinematic viscosity 12 cm^2/sec to maintain a viscosity similar to that of human blood. Fluid from an upstream tank is pumped through a straight tube that is long enough to achieve fully developed laminar flow and minimize boundary effects. After dividing at the bifurcation, fluid flows directly into a constant head tank. The phantom-fixed box can be tilted over a range of 180° (outlet side up and down, above and below the level of the pump system).

A.

B.

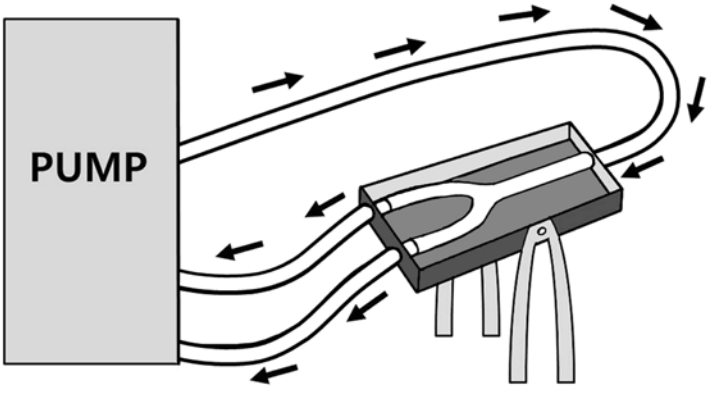

Figure1. Design of the phantom and pulsatile flow loop. (A) The silicon phantom imitating a bifurcating vessel with a thin-elastic wall at its apex (arrow). (B) Illustration of the closed loop of pulsatile flow generated by a pump and tiltable box to which the phantom is fixed.

B. Video recording of phantom experiment

Video recording was performed to record the cyclic morphological changes of the phantom in response to pulsatile flow while the phantom-fixed box was being tilted from an outlet side up position to a down position. Images were captured at the 45° up, horizontal and 90° down positions of the phantom, and the areas of evaginations were measured with a tool contained in the PACS (picture archiving communication system) program. The position of the phantom was indicated by the projections of a paper clip hanging on a string

2. Computational fluid dynamics (CFD) study

We designed three-dimensional CFD models of a bifurcating vessel (diameter ratio, inlet diameter/outlet diameter=3/2; bifurcation angle, 140°) with either rigid or compliant wall using commercially available software, CFD-ACE+ (CFD Research Corp., Huntsville, AL, USA). The details in mathematical methods are provided in the Appendix.

A total of 41,362 structured grids composed of hexahedral elements were generated to obtain reliable calculations of fluid-structure interactions and to analyze solid structure deformation in response to pressure gradients. We generated two models differing in wall compliance (rigid vs. compliant) by implementing elastic conditions in one of the two geometric conformations. For the compliant model, the implemented elastic modulus of the vessel wall was 80 kPa according to Friedman et al, and 4 kPa specifically at the apex of the bifurcation to reproduce the characteristics of medial defects.[16]

The fluid domain was assumed to be an unsteady, incompressible non-Newtonian fluid. Blood flow was mathematically modeled using the unsteady 3D Navier–Stokes equations, and the Carreau model was used to calculate the viscosity of the blood. The pulsatile flow was set according to the clinical results

of Doppler ultrasound in a normal volunteer. The boundary condition of fluid flow was the same for the compliant and non-compliant models. For the inlet boundary condition, we assigned the velocity distribution at the peak of pulsatile flow.

Thirty temporal resolutions were set within one cardiac cycle (0.8 sec). Calculations were performed for three cardiac cycles, and the results of the last cycle were used for analysis. We evaluated the hemodynamic characteristics of each model with respect to pressure, velocity and wall deformation.

II. RESULTS

1. Phantom study

In response to pulsatile flow, cyclic evagination-and-flattenings could be observed at the apex of the bifurcation of the phantom (Figure 2). During the diastolic phase, the evagination became completely flat.

The size of the evaginations increased as the outlet side of the phantom was tilted down below the level of the circulation pump system. The areas of evagination on captured images were calculated with PACS system program. As compared with outlet side 45° up position, the area of evagination increased 2.4 times in horizontal position and 3.7 times in outlet side 90° down position.

A.

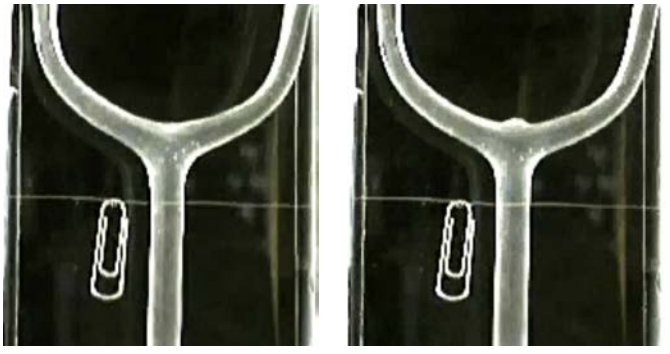

B.

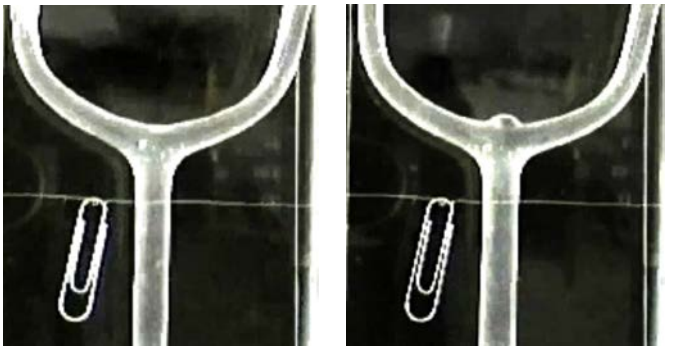

C.

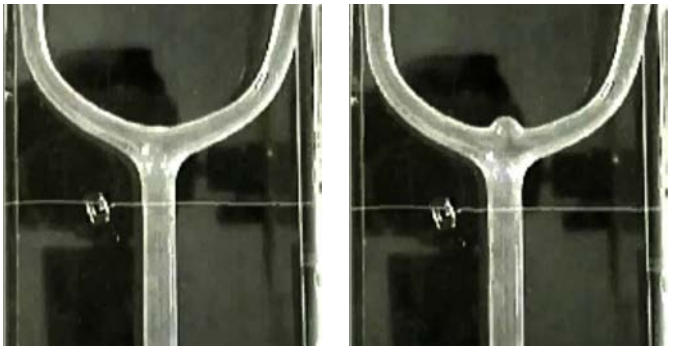

Figure 2. Capture images of phantom with outlet side 45° up (A), horizontal (B) and 90° down (C) position. Evagination-and-flattenings could be seen at the apex in response to the cyclic pulsatile flow. As the outlet side of the phantom tilted down, the size of evagination increased (B, C). The position of phantom could be indicated by the different projection of paper clip hanged on a string according to the gravity.

2. CFD study

The results of the CFD study are presented in Figures 3 and 4. At the peak-systolic phase, morphologic deformation, i.e. evagination at the bifurcation apex could be seen in the compliant model, and the pressure gradient was highest in the evagination. At the end-diastolic phase, both rigid and compliant models displayed identical hemodynamic characteristics as a function of pressure and velocity. The rigid model showed no morphological deformation throughout the cardiac cycles.

A.
B.
C.
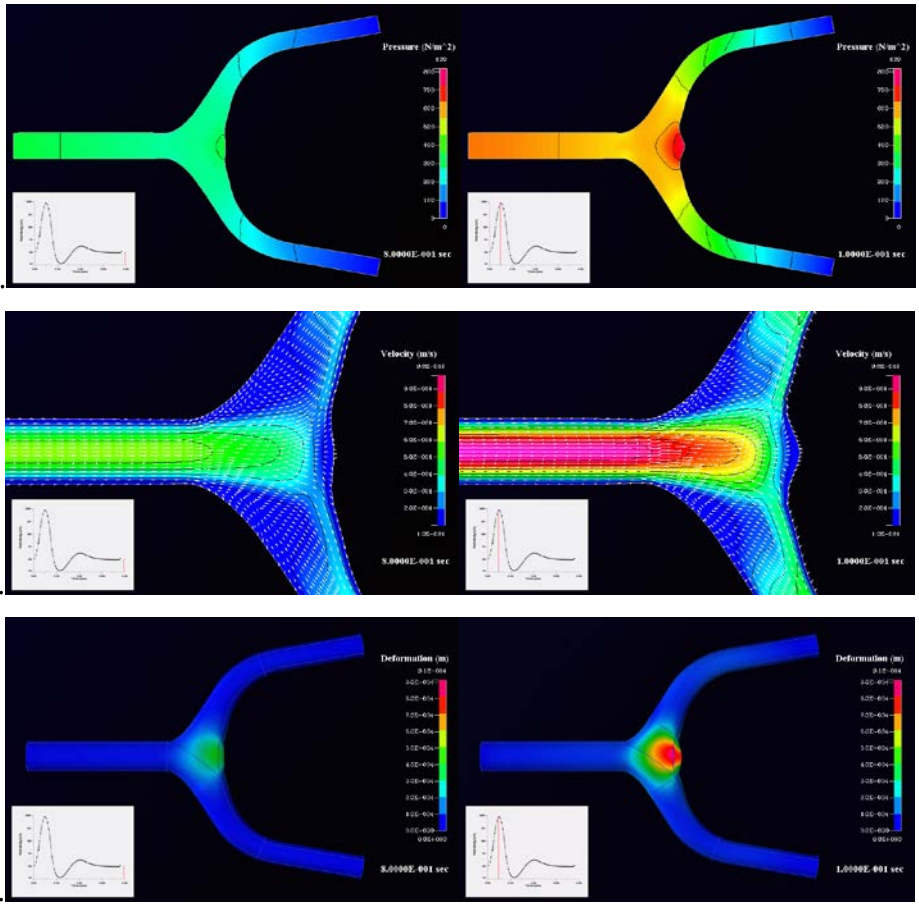

Figure 3. Results of CFD simulation of the elastic model. End-diastolic (right row) and peak systolic (left row) characteristics of pressure (A), velocity (B) and deformation (C). Morphologic deformation, i.e. evagination at the apex of the bifurcation was seen in the peak systolic phase, and the pressure gradient was highest in the evaginating apex.

A.
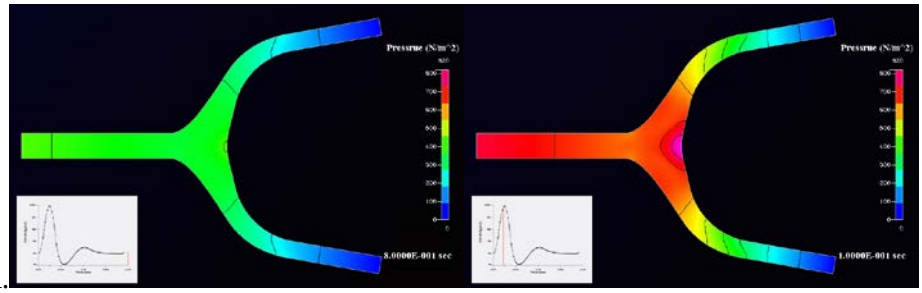

B.
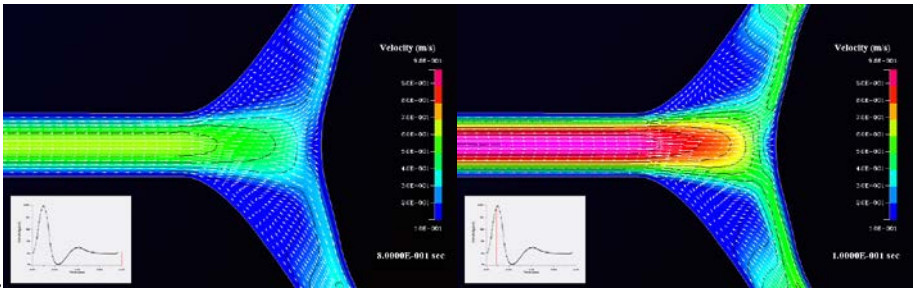

C.
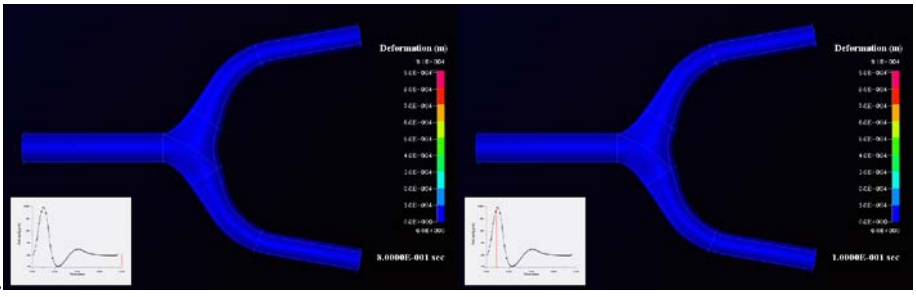

Figure 4. Results of CFD simulation of the rigid model. End-diastolic (right row) and peak systolic (left row) characteristics of pressure (A), velocity (B) and deformation (C). No morphological deformation was observed throughout the cardiac cycle.

.

IV. DISCUSSION

The natural history of intracranial aneurysms consists of genesis, growth, and rupture. It is generally accepted that the pathogenesis is associated with abnormally high hemodynamic stresses on the arterial bifurcation where complex wall shear stresses and wall shear stress gradients are observed.[17] When considering the preferential occurrence of aneurysms at arterial bifurcations, one should not underestimate the effect of the wall composition of these particular regions on the initiation of aneurysms. Hemodynamic stress activates elastase in endothelial cells leading to degeneration of the internal elastic lamina and intimal pad.[18, 19] This is very important for aneurysm formation because internal elastic lamina plays a role in the toleration of high blood pressure.[2] As a result of repeated hemodynamic stress, the apex of an arterial bifurcation may develop a wider medial defect, as well as an inelastic intimal pad and a disrupted internal elastic lamina, all of which are thought to be requisite for aneurysm formation.[20]

Pre-aneurysmal lesions have been shown to be funnel-shaped dilatations, areas of thinning and microscopic evagination with a histopathology of medial defects and degeneration of the internal elastic lamina.[20, 21] A cadaveric study of early changes in cerebral aneurysms reported that these histopathologic changes were observed significantly more often in the aneurysm series than in the control, suggesting that there may be predisposing factors in subjects with aneurysms.[20] Despite the debate about whether medial defects are congenital or acquired, the walls of cerebral artery bifurcations have varying degrees of such defects and these have a tendency to increase with age.[4] We may suppose that the medial defect is an important underlying element in the initiation of aneurysms and that hemodynamic factors may then trigger their development. The growth of an aneurysm depends on an interaction between hemodynamic loads and mechanobiologic responses of the cellular elements of the wall resulting in weakening of the wall, though there is still controversy about the role of high

versus low flow in aneurysm growth and ultimate rupture.[22]

The rationale of this study is based on our previous report of pulsatile evagination-and-flattening, i.e. a compliance zone, at the apex of the cerebral artery bifurcation demonstrated by ECG-gated MR and CT angiography in vivo.[1] We supposed that the compliance zone might be related to a regional medial defect. However, this needed to be validated by being experimentally reproduced because the hemodynamic environment of small cerebral arterial bifurcations may lead to false interpretations in TOF MR angiography.[6-10] For that purpose, we designed models having a thin-elastic apical region imitating the medial defect region of an arterial bifurcation and we were able to reproduce pulsatile evagination-and-flattening. Our results suggest that the compliance zones noted on ECG-gated MR and CT angiography are real and depend on a thin-elastic wall in the apex region. The pulsatile expansion observed on ECG-gated MR and CT angiograms could be reproduced by our phantom and CFD models having similar wall characteristics to medial defect regions. Therefore, we may presume that the compliance zones on ECG-gated angiograms are closely related to medial defects. It may also be associated with the earliest manifestation of an aneurysm, though it is not clear whether the compliance zone is a functioning normal anatomical structure or a pathologic element, i.e. a transient pre-aneurysmal structure in equilibrium between residual elasticity and on-going degeneration. As for the growth and rupture of aneurysms, CFD simulations have been used extensively to explain their mechanisms.[23] However, in contrast to full-blown aneurysms, the hemodynamics of pre-aneurysmal lesions are only partially understood because, as far as we know, there has been no reproducible model system. A longitudinal follow-up of individuals with compliance zones is required to reveal the identity of these zones, i.e. whether they develop into aneurysms or not. In the meantime, experimental reproduction and precise hemodynamic evaluation of compliance zones may be first steps in establishing their significance.

The appearance and size of evaginations in the compliance zone were closely

related to the pressure gradient of pulsatile flow. This could be demonstrated in our phantom as enlargement of the evagination when the outlet side was tilted below the level of the pump system. We thought that the gravity made stagnation of the flow in the phantom resulting in an increase of hydraulic pressure.

We focused on aneurysms at cerebral artery bifurcations with approximately symmetric angles and diameters of the distal branches. Diverse geometries of parent vessel, take-off angle of daughter vessels and ratios of daughter vessel diameters may affect the site, direction and growth of aneurysms because of different wall shear stresses on the wall.[24] The side wall aneurysms of internal carotid artery such as posterior communicating artery aneurysms or paraclinoid aneurysms also accompany daughter vessels near at the origin, unless they are associated with dissection or other causative diseases. This may suggest that medial defects are also related to the formation of side wall aneurysms though with quite a large discrepancy in diameter compared to parent vessels. Phantoms or CFD models with various combinations of parent vessel geometries, daughter vessel take-off angles and daughter diameter ratios should be designed for the full understanding of hemodynamics in aneurysmal genesis.

V. CONCLUSIONS

We have reproduced the compliance zones at arterial bifurcations in the form of regions of pulsatile evagination-and-flattening in a phantom experiment and CFD simulations. Their appearance in thin-elastic apical regions suggests that compliance zones are closely related to the well-known histopathologic characteristics of the apices of cerebral artery bifurcations, i.e. medial defects. This implies that the compliance zone is a real and reproducible anatomical structure. Our phantom and CFD models should provide starting points for further investigations aimed at understanding the initiation of cerebral aneurysms.

REFERENCES

1. Lee YJ, Chung TS, Rhim YC, Suh SH, Foo TK. Echocardiogram-gated computed tomographic and magnetic resonance angiographies for the detection of pulsatile expansion at the intracranial arterial bifurcation. Journal of computer assisted tomography 2010;34(6):842-6.
2. Glynn LE. Medial defects in the circle of Willis and their relation to aneurysm formation. J Pathol Bacteriol 1940;51:213-22.
3. Fujimoto K. 'Medial defects' in the prenatal human cerebral arteries: an electron microscopic study. Stroke; a journal of cerebral circulation 1996;27(4):706-8.
4. Stehbens WE. Medial defects of the cerebral arteries of man. J Pathol Bacteriol 1959;78:179-85.
5. Canham PB, Finlay HM. Morphometry of medial gaps of human brain artery branches. Stroke; a journal of cerebral circulation 2004;35(5):1153-7.
6. Chung TS, Lee YJ, Kang WS, Kang SK, Rhim YC, Yoo BG, et al. Clinical and experimental investigation of pseudoaneurysm in the anterior communicating artery area on 3-dimensional time-of-flight cerebral magnetic resonance angiography. Journal of computer assisted tomography 2004;28(3):414-21.
7. Anderson CM, Saloner D, Tsuruda JS, Shapeero LG, Lee RE. Artifacts in maximum-intensity-projection display of MR angiograms. AJR American journal of roentgenology 1990;154(3):623-9.
8. Okahara M, Kiyosue H, Yamashita M, Nagatomi H, Hata H, Saginoya T, et al. Diagnostic accuracy of magnetic resonance angiography for cerebral aneurysms in correlation with 3D-digital subtraction angiographic images: a study of 133 aneurysms. Stroke; a journal of cerebral circulation 2002;33(7):1803-8.
9. Kemmling A, Noelte I, Gerigk L, Singer S, Groden C, Scharf J. A diagnostic pitfall for intracranial aneurysms in time-of-flight MR angiography: small intracranial lipomas. AJR American journal of roentgenology 2008;190(1):W62-7.
10. Wilcock DJ, Jaspan T, Worthington BS. Problems and pitfalls of 3-D TOF magnetic resonance angiography of the intracranial circulation. Clinical radiology 1995;50(8):526-32.
11. Raschi M, Mut F, Byrne G, Putman CM, Tateshima S, Vinuela F, et al. CFD and PIV Analysis of Hemodynamics in a Growing Intracranial Aneurysm. International journal for numerical methods in biomedical engineering 2012;28(2):214-28.

12. Cebral JR, Pergolizzi RS, Jr., Putman CM. Computational fluid dynamics modeling of intracranial aneurysms: qualitative comparison with cerebral angiography. Academic radiology 2007;14(7):804-13.
13. Steinman DA, Vorp DA, Ethier CR. Computational modeling of arterial biomechanics: insights into pathogenesis and treatment of vascular disease. J Vasc Surg 2003;37(5):1118-28.
14. van Ooij P, Guedon A, Poelma C, Schneiders J, Rutten MC, Marquering HA, et al. Complex flow patterns in a real-size intracranial aneurysm phantom: phase contrast MRI compared with particle image velocimetry and computational fluid dynamics. NMR in biomedicine 2012;25(1):14-26.
15. Ford MD, Nikolov HN, Milner JS, Lownie SP, Demont EM, Kalata W, et al. PIV-measured versus CFD-predicted flow dynamics in anatomically realistic cerebral aneurysm models. Journal of biomechanical engineering 2008;130(2):021015.
16. Friedman MH, Bargeron CB, Duncan DD, Hutchins GM, Mark FF. Effects of arterial compliance and non-Newtonian rheology on correlations between intimal thickness and wall shear. Journal of biomechanical engineering 1992;114(3):317-20.
17. Meng H, Swartz DD, Wang Z, Hoi Y, Kolega J, Metaxa EM, et al. A model system for mapping vascular responses to complex hemodynamics at arterial bifurcations in vivo. Neurosurgery 2006;59(5):1094-100; discussion 100-1.
18. Cajander S, Hassler O. Enzymatic destruction of the elastic lamella at the mouth of cerebral berry aneurysm? An ultrastructural study with special regard to the elastic tissue. Acta neurologica Scandinavica 1976;53(3):171-81.
19. Stehbens WE, Ludatscher RM. Ultrastructure of the renal arterial bifurcation of rabbits. Exp Mol Pathol 1973;18(1):50-67.
20. Kayembe KN, Kataoka H, Hazama F. Early changes in cerebral aneurysms in the internal carotid artery/posterior communicating artery junction. Acta Pathol Jpn 1987;37(12):1891-901.
21. Stehbens WE. Histopathology of cerebral aneurysms. Archives of neurology 1963;8:272-85.
22. Cebral JR, Mut F, Weir J, Putman C. Quantitative characterization of the hemodynamic environment in ruptured and unruptured brain aneurysms. AJNR American journal of neuroradiology 2011;32(1):145-51.
23. Farnoush A, Avolio A, Qian Y. Effect of Bifurcation Angle Configuration and Ratio of Daughter Diameters on Hemodynamics of Bifurcation Aneurysms. AJNR American journal of neuroradiology 2013;34(2):391-6.

24. Mantha A, Karmonik C, Benndorf G, Strother C, Metcalfe R. Hemodynamics in a cerebral artery before and after the formation of an aneurysm. AJNR American journal of neuroradiology 2006;27(5):1113-8.

APPENDICES

I. Computational Fluid Dynamics model design

1. A total of 41,362 structured grids composed of hexahedral elements were generated for the reliable calculation of fluid-structure interaction and for the analysis of solid structure deformation corresponding to the pressure gradient.

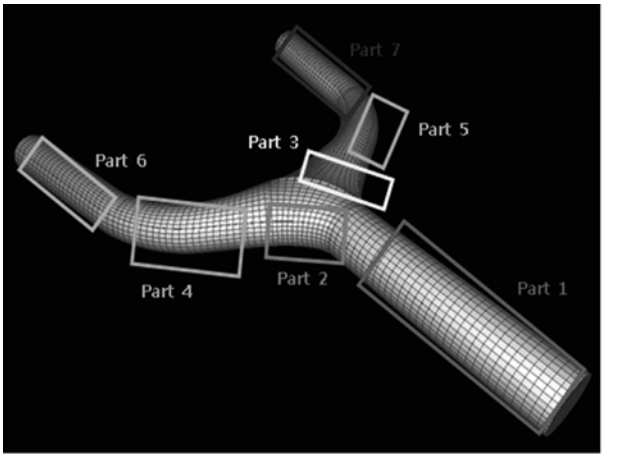

Grid information of CFD model

Part name	Part #	# of Cell	# of Fluid Cell	# of Solid Cell
Parent artery	Part 1	7,680	5,504	2,176
Daughter artery	Part 5	6,984	5,064	1,920
	Part 7	6,984	5,064	1,920
Daughter artery	Part 4	5,760	4,128	1,632
	Part 6	5,760	4,128	1,632
Bifurcating part	Part 2	2,665	1,963	702
	Part 3	5,529	4,009	1,520
SUM		41,362	29,860	11,502

2. We designed butterfly shaped-structural block meshes composed of a central fluid block surrounded by four fluid blocks and another four solid blocks in the outermost layer. Each block has six faces with an equal number of grids in the opposing faces.

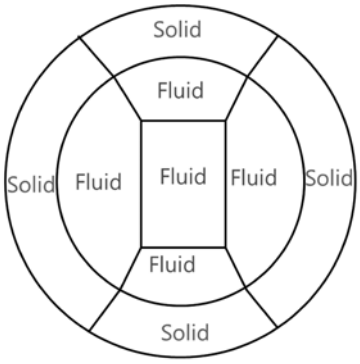

3. For the analysis of shear distribution and wall deformation of compliant model, finite element method was used. The density of vessel wall was set as 1,030 kg/m^3.
4. Fluid domain was assumed as unsteady, incompressible non-Newtonian fluid and the governing equations were continuity equation, low of conservation of momentum, and Navier-Stokes equation. Carreau model was used for the calculation of the viscosity of blood. The pulsatile flow was set by the clinical result with Doppler ultrasound of normal volunteer. The boundary condition of fluid flow was equally assigned for both compliant and non-compliant model. For inlet boundary condition, velocity distribution at the peak point of pulsatile flow was assigned.

Inlet fluid velocity (function of time and place) :

The equation with Fourier series × parabolic velocity profile

$$\boldsymbol{U}(\boldsymbol{r},\boldsymbol{t}) = \boldsymbol{v}_{\boldsymbol{axis}-\max}(1-\boldsymbol{k}\,\boldsymbol{r}^2)\cdot(\frac{\boldsymbol{a}_0}{2}+\sum_{\boldsymbol{i}=1}^{10}\boldsymbol{a}_i\cos(\boldsymbol{\omega}\boldsymbol{t})+\boldsymbol{b}_i\sin(\boldsymbol{\omega}\boldsymbol{t}))$$

r : distance from axis

k: 1/r2 to provide no slip condition and zero velocity at the wall

II. Computational Fluid Dynamics Analysis

1. Formulas for CFD analysis of hemodynamics of unsteady, incompressible, non-Newtonian fluid in three-dimensional compliant vessel,

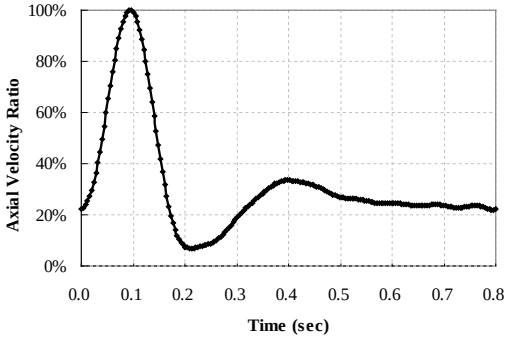

$$\nabla \bullet \vec{\boldsymbol{V}} = 0$$

$$\boldsymbol{\rho}\left(\frac{\partial \vec{\boldsymbol{V}}}{\partial \boldsymbol{t}} + \vec{\boldsymbol{V}} \bullet \nabla \vec{\boldsymbol{V}}\right) = -\nabla \boldsymbol{p} + \boldsymbol{\rho}\vec{\boldsymbol{g}} + \boldsymbol{\mu}\nabla^2 \vec{\boldsymbol{V}}$$

$$\boldsymbol{\mu} = \boldsymbol{\mu}_\infty + (\boldsymbol{\mu}_0 - \boldsymbol{\mu}_\infty)\left[1 + (\boldsymbol{\lambda}\dot{\boldsymbol{\gamma}})^2\right]^{\frac{\boldsymbol{n}-1}{2}}$$

ρ: density of blood, 1,020 kg/m3

V: 3 demensional velocity vector of fluid

P: static pressure of blood

∇: operator $\left[\frac{\partial}{\partial \boldsymbol{x}}(\ )\boldsymbol{i} + \frac{\partial}{\partial \boldsymbol{y}}(\ )\boldsymbol{j} + \frac{\partial}{\partial \boldsymbol{z}}(\ )\boldsymbol{k}\right]$

∇2: operator $\left[\frac{\partial^2}{\partial \boldsymbol{x}^2}(\ )\boldsymbol{i} + \frac{\partial^2}{\partial \boldsymbol{y}^2}(\ )\boldsymbol{j} + \frac{\partial^2}{\partial \boldsymbol{z}^2}(\ )\boldsymbol{k}\right]$

μ: apparent viscosity of blood

Constants in Carreau model.

Constants	Constant name	value
μ	Apparent viscosity	Implicit
μ_∞	Infinite-shear-rate viscosity	$3.45e-6N\cdot s/m^2$
μ_0	Zero-shear-rate viscosity	$5.6e-5N\cdot s/m^2$
λ	Time constant	3.313s
$\dot{\gamma}$	Shear rate	0.356

2. Upwind scheme was used for Numeric analysis for fluid flow.
3. For the correction of velocity and pressure, Semi-Implicit Method for Pressure Linked Equations (SIMPLE) algorithm method was used.
4. For the calculation of stress, Direct solver was used.
5. The Elastic Modulus was assigned as 4 *kPa* at the bifurcation region and 80 *kPa* at the remainder.
6. After calculation of wall pressure in the non-compliant vessel by flow solver, the deformation of each element was calculated by stress solver with that pressure and material property of given vessel. When the both pressure from flow solver and stress solver became equal and corresponding deformation converged to a certain value by repetition of this process, we stopped the calculation and analyzed the static deformation of bifurcating vessel.

ABSTRACT(IN KOREAN)

뇌동맥 분지부 컴플라이언스 영역의 실험 규명 : 팬텀 및 전산유체역학 시뮬레이션의 비교연구

<지도교수 정 태 섭>

연세대학교 대학원 의학과

이 영 준

저자들은 이전 연구에서 심전도-동기 CT, MR 혈관조영술을 이용하여 뇌혈관분지부의 첨부에서 박동성 혈류에 순응하여 미세돌출-납작해짐이 반복되는 컴플라이언스 영역이 관찰될 수 있음을 보고하였다. 본 연구는 이 컴플라이언스 영역의 존재를 실험적으로 재현해서 입증하고, 이 영역과 얇고 탄성있는 혈관벽과의 연관성을 알아보고자 하였다.

혈관분지부에 탄성영역을 가지는 형태의 혈관 모형으로 팬텀 실험 및 전산유체역학 (CFD) 시뮬레이션을 수행 하였다.

팬텀의 첨부에서 박동성 순환 혈류에 따른 컴플라이언스 영역을 재현할 수 있었다. 팬텀의 출구 쪽을 낮게 기울였을 때 미세돌출 부의 크기가 증가하였다. CFD 시뮬레이션에서도 첨부에 탄성이 있는 모델에서 컴플라이언스 영역이 재현되었고 동맥기에서 컴플라이언스 영역에 가장 높은 압력분포가 관찰되었다.

저자들은 실험적으로 컴플라이언스 영역을 재현하였다. 이 영역은 얇고 탄성있는 혈관벽 부위와 일치하였으며 압력에 비례하여 반응하였다.

핵심되는 말 : 동맥류, 전산유체역학, 팬텀, 컴플라이언스

PUBLICATION LIST

1. Chung TS, Lee YJ, Kang WS, Kang SK, Rhim YC, Yoo BG, et al. Clinical and experimental investigation of pseudoaneurysm in the anterior communicating artery area on 3-dimensional time-of-flight cerebral magnetic resonance angiography. Journal of computer assisted tomography. 2004;28:414-21

2. Lee YJ, Chung TS, Rhim YC, Suh SH, Foo TK. Echocardiogram-gated computed tomographic and magnetic resonance angiographies for the detection of pulsatile expansion at the intracranial arterial bifurcation. Journal of computer assisted tomography. 2010;34:842-6